

Molecular interpretation of the non-Newtonian viscoelastic behavior of liquid water at high frequencies

Julius C. F. Schulz,¹ Alexander Schlaich^{1,2}, Matthias Heyden^{1,3}, Roland R. Netz,¹
and Julian Kappler^{1,4,*}

¹*Freie Universität Berlin, Fachbereich Physik, 14195 Berlin, Germany*

²*Université Grenoble Alpes, CNRS, LIPhy, 38000 Grenoble, France*

³*School of Molecular Sciences and Center for Biological Physics, Arizona State University,
Tempe, Arizona 85287-1604, USA*

⁴*Department of Applied Mathematics and Theoretical Physics, University of Cambridge,
Cambridge CB3 0WA, United Kingdom*



(Received 5 May 2020; accepted 10 September 2020; published 14 October 2020)

Using classical as well as *ab initio* molecular dynamics simulations, we calculate the frequency-dependent shear viscosity of pure water and water–glycerol mixtures. In agreement with recent experiments, we find deviations from Newtonian-fluid behavior in the THz regime. Based on an extension of the Maxwell model, we introduce a viscoelastic model to describe the observed viscosity spectrum of pure water. We find four relaxation modes in the spectrum which we attribute to (i) hydrogen–bond network topology changes, (ii) hydrogen–bond stretch vibrations of water pairs, (iii) collective vibrations of water molecule triplets, and (iv) librational excitations of individual water molecules. Our model quantitatively describes the viscoelastic response of liquid water on short timescales, where the hydrodynamic description via a Newtonian-fluid model breaks down.

DOI: [10.1103/PhysRevFluids.5.103301](https://doi.org/10.1103/PhysRevFluids.5.103301)

I. INTRODUCTION

Liquid water is an ubiquitous medium on earth and of fundamental importance for all organisms [1,2]. A standard model for the large-scale hydrodynamics of liquid water is the Newtonian fluid [3–5], where one assumes a linear relationship between local instantaneous stresses and rates of strain, with the proportionality constant given by the viscosity. The combination of the momentum conservation equation with this relation is then known as the Navier–Stokes equation, and it is the basis for hydrodynamics.

Despite its success for describing the dynamics of water and other liquids, this model has a limited range of applicability. At high frequencies, when timescales are comparable to those of molecular kinetics within the liquid, real water deviates from the Newtonian fluid model. Slie *et al.* [6] showed by ultrasound absorption measurements that in aqueous glycerol solutions, the shear viscosity decreases and the mixture starts to have an elastic response under shear deformation at high frequencies. More recently, Pelton *et al.* [7] showed that the same occurs for pure water. Both studies replaced the Newtonian fluid model by a viscoelastic Maxwell fluid [8], which in the low frequency limit reduces to a Newtonian fluid but can account for the experimentally observed elastic behavior at high frequencies. Molecular dynamics simulations of water–glycerol mixtures [9] and pure water [10,11] also find a non-Newtonian regime at high frequencies, the onset of which is well-described by a Maxwell model [9,11].

*jkappler@posteo.de

Understanding this non-Newtonian behavior is becoming increasingly important. First, with the advancement of nanotechnology, small structures, when in an aqueous environment, start to probe the regime where the Newtonian-fluid model of water breaks down [7,12,13]. Second, the THz regime probed by modern spectroscopic methods constitutes the boundary between collective and single-water dynamics [13–19]. If one seeks detailed insight into dynamics of molecular or collective processes of solutes on such fast timescales, an important aspect is therefore understanding how water itself behaves on the relevant time- and length scales.

In the present work, we use both force-field molecular dynamics (MD) and *ab initio* molecular dynamics (aiMD) simulations to probe the high-frequency behavior of both pure water and water-glycerol mixtures. From our simulations, we extract the frequency-dependent shear viscoelasticity. We verify our method by comparing to the experimental results of Slie *et al.* [6] for the viscoelasticity of water-glycerol mixtures. Then we investigate the MD spectrum of pure water in more detail. We propose a viscoelastic model to account for deviations of the observed water viscosity spectrum from the Maxwell model. We identify four independent relaxation modes in the THz regime and link them to molecular processes, namely, (i) hydrogen-bond network topology changes, (ii) hydrogen-bond stretch vibrations, (iii) collective vibrations of water molecule triplets, (iv) librational excitations of individual water molecules. We validate the use of classical force-field MD simulations by comparing to a viscosity spectrum based on aiMD simulations, which shows the same high-frequency features as the spectrum obtained from force-field MD simulations. The aiMD spectrum additionally contains features originating from intramolecular degrees of freedom (OH stretching, OH bending) at high frequencies, which are not included in the rigid water model used for the force-field MD simulations.

II. FREQUENCY-DEPENDENT VISCOSITIES

In this section we recall some generalizations of the standard Green-Kubo relation for the shear viscosity [20–25]. These generalizations can be used to calculate the frequency- and wave number dependent shear viscosity in terms of velocity and stress tensor correlation functions. Detailed derivations can be found in the Supplemental Material (SM) [26] as well as in the literature [21–23].

We start from the linearized continuum-mechanical momentum conservation equation [8], which at position \mathbf{x} and time t is given by

$$\rho \dot{v}_\alpha(\mathbf{x}, t) = \sum_{\beta=1}^3 \partial_\beta \sigma_{\alpha\beta}(\mathbf{x}, t), \quad \alpha \in \{x, y, z\}, \quad (1)$$

where ρ is the constant equilibrium mass density of the fluid, $\mathbf{v} = (v_x, v_y, v_z)$ its velocity field, σ its stress tensor, and the dot denotes a time derivative. Note that while for a compressible fluid the density is not constant, deviations from the constant equilibrium mass density ρ on the left-hand side of Eq. (1) would constitute nonlinear effects and are therefore not considered in our linear treatment. For a linear, homogeneous, isotropic compressible fluid the stress tensor is given as

$$\begin{aligned} \sigma_{\alpha\beta}(\mathbf{x}, t) = & -\delta_{\alpha\beta} P(\mathbf{x}, t) + 2 \iint \eta(|\mathbf{x}'|, t') \dot{\epsilon}_{\alpha\beta}(\mathbf{x} - \mathbf{x}', t - t') d^3 \mathbf{x}' dt' \\ & + \delta_{\alpha\beta} \sum_{\gamma=1}^3 \iint \left(\eta'(|\mathbf{x}'|, t') - \frac{2}{3} \eta(|\mathbf{x}'|, t') \right) \dot{\epsilon}_{\gamma\gamma}(\mathbf{x} - \mathbf{x}', t - t') d^3 \mathbf{x}' dt', \end{aligned} \quad (2)$$

where P is the pressure, η , η' are the shear and volume viscosity kernels, which for an isotropic medium only depend on the modulus of the vector \mathbf{x}' , $\delta_{\alpha\beta}$ is the Kronecker delta, and the components of the rate of strain tensor $\dot{\epsilon}$ are

$$\dot{\epsilon}_{\alpha\beta} = \frac{1}{2} \left(\frac{\partial v_\alpha}{\partial x_\beta} + \frac{\partial v_\beta}{\partial x_\alpha} \right), \quad \alpha, \beta \in \{x, y, z\}. \quad (3)$$

If the viscosity kernels decay on length- and timescales that are small compared to those on which the rate of strain tensor varies, then the stress tensor defined by Eq. (2) can be approximated as [26]

$$\sigma_{\alpha\beta}(\mathbf{x}, t) \approx -\delta_{\alpha\beta}P(\mathbf{x}, t) + 2\bar{\eta}\dot{\epsilon}_{\alpha\beta}(\mathbf{x}, t) + \delta_{\alpha\beta}\left(\bar{\eta}' - \frac{2}{3}\bar{\eta}\right)\sum_{\gamma=1}^3\dot{\epsilon}_{\gamma\gamma}(\mathbf{x}, t), \quad (4)$$

where

$$\bar{\eta} = \iint \eta(|\mathbf{x}'|, t') d^3\mathbf{x}' dt', \quad (5)$$

$$\bar{\eta}' = \iint \eta'(|\mathbf{x}'|, t') d^3\mathbf{x}' dt', \quad (6)$$

are the standard shear and volume viscosities, which do not depend on space and time. A fluid with stresses given by Eq. (4) is called a Newtonian fluid. If the stress tensor Eq. (4) is used in the momentum conservation Eq. (1), then the linearized compressible Navier–Stokes equation is recovered. While in this work we mostly consider the spatial average of the shear viscosity kernel, we are precisely interested in the dynamics on timescales where the approximation Eq. (4) breaks down, and non-Markovian effects become relevant.

From momentum conservation Eqs. (1) and (2), and the equipartition theorem, it follows that the shear viscosity kernel η is given in terms of the trace free part of the stress tensor,

$$\Pi_{\alpha\beta} = \sigma_{\alpha\beta} - \delta_{\alpha\beta} \frac{1}{3} \sum_{\gamma} \sigma_{\gamma\gamma} \quad \alpha, \beta \in \{x, y, z\}, \quad (7)$$

as [22,24–26]

$$\tilde{\eta}(\mathbf{k} = 0, \omega) = \frac{\beta V}{10} \int_0^{\infty} e^{-i\omega t} \sum_{\alpha\beta} \langle \Pi_{\alpha\beta}(t) \Pi_{\alpha\beta}(0) \rangle dt, \quad (8)$$

where V is the volume of the fluid, $\beta^{-1} = k_B T$ is the thermal energy with k_B the Boltzmann constant and T the absolute temperature, the tilde denotes a combined spatial Fourier transform (with wave vector \mathbf{k}) and temporal half-sided Fourier transform (with angular frequency ω), and the average on the right-hand side denotes an ensemble average over space. The real part of $\tilde{\eta}$ yields the viscous response under shear, whereas the imaginary part models the elastic response under shear [8].

Note that, in view of Eqs. (4) and (5), $\tilde{\eta}$ evaluated at $\mathbf{k} = 0$ can be thought of as the viscosity for a viscosity kernel that decays on a length scale much smaller than the length scale on which $\dot{\epsilon}$ varies, but including memory effects in time. If additionally the limit $\omega \rightarrow 0$ is taken, memory effects in time are also neglected and the Green-Kubo relation for $\bar{\eta}$ is obtained from Eq. (8) as [20–25,27]

$$\bar{\eta} = \frac{\beta V}{10} \int_0^{\infty} \sum_{\alpha\beta} \langle \Pi_{\alpha\beta}(t) \Pi_{\alpha\beta}(0) \rangle dt. \quad (9)$$

In this paper we use Eqs. (8) and (9) to calculate the viscosity based on force–field MD simulations, where the space-averaged pressure tensor is available [28]. To calculate shear viscosities from the aiMD simulations, we use that for small wave number $k = |\mathbf{k}|$, the shear viscosity is given by [21–23,26]

$$\tilde{\eta}(k, \omega) = -\frac{\rho}{k^2} \int_0^{\infty} e^{-i\omega t} \ddot{C}^{\perp}(k, t) dt, \quad (10)$$

where a hat denotes a spatial Fourier transform and \hat{C}^\perp is the normalized autocorrelation function of the α -component of the transversal velocity,

$$\hat{C}^\perp(k, t) = \frac{\langle \hat{v}_\alpha^\perp(\mathbf{k}, t) \hat{v}_\alpha^\perp(-\mathbf{k}, 0) \rangle}{\langle \hat{v}_\alpha^\perp(\mathbf{k}, 0) \hat{v}_\alpha^\perp(-\mathbf{k}, 0) \rangle}, \quad \alpha \in \{x, y, z\}, \quad (11)$$

with $\hat{v}_\alpha^\perp := \sum_\beta (\delta_{\alpha\beta} - k_\alpha k_\beta / k^2) \hat{v}_\beta$ the components of the transversal velocity. For an isotropic medium, the right-hand side of Eq. (11) does not depend on the component α used and only depends on \mathbf{k} via the modulus k , which is why \hat{C}^\perp has no index α and is written as a function of k .

In the context of Eq. (10), small wave number means [26]

$$\left| \frac{k^2 \tilde{\eta}}{\rho \omega} \right| \ll 1, \quad (12)$$

which for realistic values for water, $|\tilde{\eta}| \approx 1 \text{ mPa s}$, $\rho = 10^3 \text{ kg/m}^3$, gives $|k|^2 \text{ nm}^2 / \text{ps} \ll |\omega|$. Thus, for $|k| = 4 \text{ nm}^{-1}$, corresponding to the smallest wave number resolvable in a typical box in an aiMD simulation, Eq. (10) is valid for $f = \omega / (2\pi) \gg 2.5 \text{ THz}$, which severely limits the applicability of Eq. (10). While in the limit $\mathbf{k} \rightarrow 0$, condition Eq. (12) is always fulfilled and the approximate Eq. (10) is valid, obtaining $\hat{v}_\alpha^\perp(\mathbf{k} = 0, t)$ from simulations is typically difficult because large simulation boxes are needed to resolve small wave numbers, and thereby to extrapolate to $\mathbf{k} = 0$. In this context it is also important to note that for a nonperiodic box so small that Eq. (12) is violated for the smallest wave numbers accessible, confinement-dependent deviations from bulk behavior start to become relevant [12], underscoring the importance of the inequality Eq. (12) at finite \mathbf{k} .

III. GLYCEROL SPECTRA

We simulate glycerol solutions [29] with glycerol mass fractions 0, 0.2, 0.4, 0.6, 0.8 in TIP4P/2005 water, for details see SM [26]. From the simulations we calculate the respective viscosity spectra at $\mathbf{k} = 0$ using Eq. (8). The resulting spectra are shown as blue and green solid curves in Fig. 1.

For low frequencies, the real parts (blue solid lines) of the spectra are constant and the imaginary parts (green solid lines) vanish. As the frequency is increased, the real parts of the spectra decrease to zero, while the imaginary parts show peaks. For low glycerol mass fractions, the real part of the shear viscosity shows a non-monotonic behavior with a second peak at around 10 THz, accompanied by a peak in the imaginary part at slightly higher frequencies. For large glycerol mass fractions, this high-frequency peak disappears, and the decay in the real part with its corresponding peak in the imaginary part shift to lower frequencies.

These spectra illustrate the limits of the Newtonian fluid model, as defined by Eq. (4), because for such a fluid one would expect a spectrum with constant real part and vanishing imaginary part over the whole frequency range. Our spectra exhibit deviations from this behavior for high frequencies, indicating that the assumption of temporal locality breaks down once the rate of strain tensor varies on the picosecond timescale, as observed in experiments [6,30] and previous numerical results [9].

To go beyond Newtonian hydrodynamics, we fit Maxwell models, defined by

$$\tilde{\eta}(\omega) = \frac{\eta_0}{1 - i\omega\tau}, \quad (13)$$

with $\eta_0 = \tilde{\eta}(0)$ the steady-state shear viscosity and a timescale τ , to the frequency range $\omega < 1 \text{ THz}$ of the glycerol-water spectra, see Fig. 1. In Fig. 2, we compare the fitted viscosities and relaxation times η_0, τ to experimental results [6,30]. As can be seen, the viscosity spectrum of the simulated glycerol/water mixtures reproduces very well both the low-frequency shear viscosity η_0 and the timescale τ for the Maxwell model. In subplot (a) we additionally include the zero-frequency viscosity, calculated using the Green-Kubo formula Eq. (9), which for pure water is in good agreement with previous numerical results [31]. The good agreement between experimental data

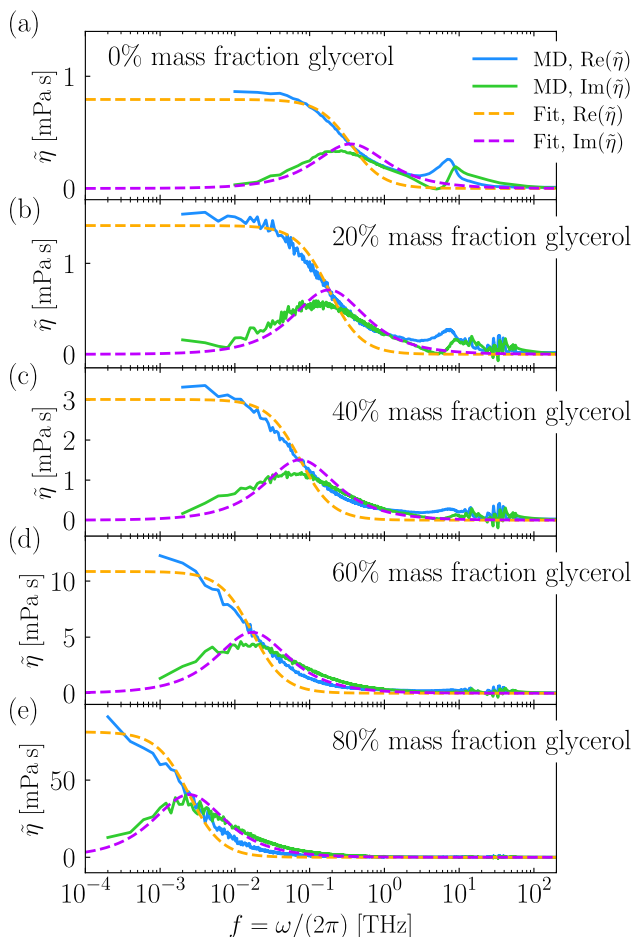


FIG. 1. Viscosity spectra $\tilde{\eta}$ as calculated from MD simulations of TIP4P/2005 water at different glycerol concentrations. The real and imaginary parts of the spectra (blue and green solid lines) are calculated from the MD data at $\mathbf{k} = 0$ using Eq. (8). The result of a Maxwell model fit, cf., Eq. (13), to frequencies 10^{-4} THz $< f < 1$ THz, is shown as orange and violet dashed lines.

and our Maxwell model fits serves as a validation that our approach of using Eq. (8) in conjunction with force–field MD simulations yields physically meaningful results.

We now demonstrate that the locations of the Maxwell-model peaks in Fig. 1 correspond to the respective timescale on which the fluid molecules rearrange. For each mass fraction of glycerol we consider the mean-squared displacement (MSD) of an individual water molecule, which we show in Fig. 3(a), together with the fitted Maxwell-model timescales τ . From Fig. 3(a) we observe that τ is the timescale on which the MSD enters its long-time diffusive scaling $\text{MSD} \propto t$. This can be seen even more clearly in Fig. 3(b), where we rescale time by the respective τ and normalize each MSD by its long-time diffusive behavior, $\text{MSD} = 6D_\infty t$, which defines the long-time diffusion coefficient D_∞ . In the representation Fig. 3(b), all the MSDs collapse onto each other for $t \gtrsim \tau$ and reach their asymptotic long-time behavior on a timescale slightly larger than τ . This shows that on timescales $t \gg \tau$ the dynamics of a fluid particle can be considered as freely diffusive, meaning that τ is the typical timescale on which fluid molecules rearrange. Correspondingly, for each glycerol mass fraction, after a time $t = \tau$ a water molecule, has traveled on average a distance comparable

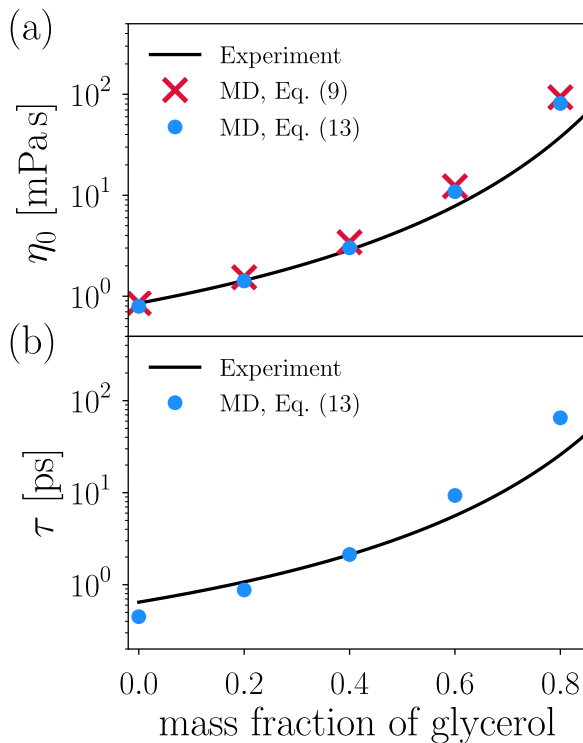


FIG. 2. Comparison of experimental and simulation data for the viscoelasticity of glycerol solutions. MD data points are obtained using the Green-Kubo formula Eq. (9) (red crosses), or fitting a Maxwell model Eq. (13) to the full viscosity spectra (blue dots), cf., Fig. 1. Experimental data for η_0 are taken from Cheng [30], timescales are calculated using $\tau = \eta_0/K$, with η_0 taken from Cheng [30] and K taken from Slie *et al.* [6]

to its own size, which is of the order of $3 \text{ \AA} = 0.3 \text{ nm}$. Indeed, in Fig. 3(a) at $t = \tau$ the value of each MSD is between $(0.2 \text{ nm})^2$ and $(0.5 \text{ nm})^2$, as indicated by a gray shaded region. The Maxwell peaks in Fig. 1 thus indicate the crossover from the solid-like short-time dynamics of the fluid, observed for frequencies higher than the Maxwell peak, to the freely-diffusive long-time dynamics, observed for frequencies lower than the Maxwell peak. This interpretation is in full agreement with the established fact that at sufficiently high frequencies, any molecular liquid is expected to behave like an (amorphous) solid [21,32,33]. Additionally, for a Yukawa liquid, a Maxwell-model peak was recently linked to nearest-neighbor escape barrier hopping within the fluid [34,35], with the peak frequency corresponding to the inverse lifetime of the nearest-neighbor topology of a given molecule. A more detailed analysis of the crossover from solid-like- to liquid-like behavior for glycerol mixtures is possible by analyzing the first-passage dynamics for dissociation of bonded water pairs [36] in glycerol solutions, or by considering collective variables that capture the locality of vibrational modes [37].

Taking a closer look at the pure TIP4P/2005 water spectrum [38], shown in Fig. 1(a), which is very similar to the previously obtained viscosity spectrum using the TIP4P force field [10], it transpires that a single Maxwell model, which features a monotonically decreasing real part and one peak in the imaginary part, is not able to model the full viscosity spectrum observed in the MD simulation, which contains two peaks in the imaginary part and a non-monotonic real part. A Maxwell model only describes this spectrum for frequencies $f \lesssim 1 \text{ THz}$, as was noted before [11].

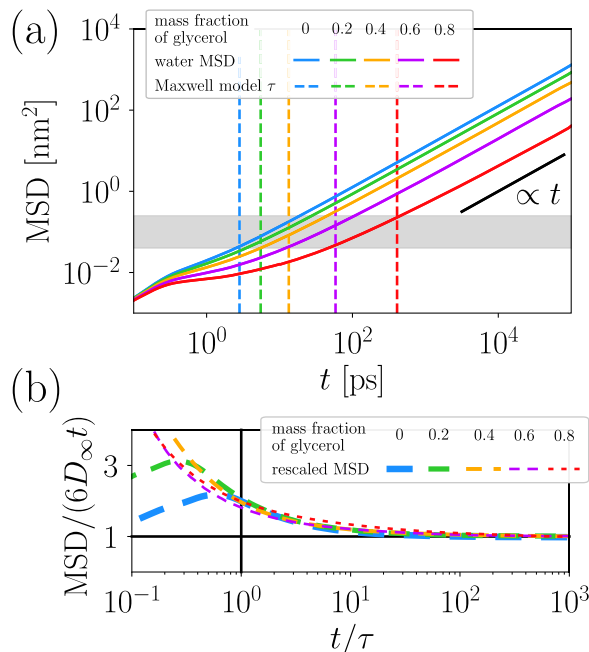


FIG. 3. Mean-squared displacement (MSD) of individual water molecules in glycerol solutions. (a) For each glycerol mass fraction, the MSD of each water molecule center of mass is calculated and an average over all such MSDs is performed (colored solid lines). The vertical dashed lines denote the corresponding fitted Maxwell-model timescales τ from Fig. 2(b), the horizontal gray shaded region denotes the range $[0.2^2 \text{ nm}^2, 0.5^2 \text{ nm}^2]$. The long-time diffusion coefficient D_∞ , defined by $\text{MSD} = 6D_\infty t$ for t large enough, is obtained from each curve by fitting a linear function to each dataset for the time interval $t/\text{ps} \in [5 \times 10^4, 10^5]$. (b) The colored lines show the MSDs from subplot (a) divided by the respective long-time diffusive MSD, and with time rescaled by the respective Maxwell timescale τ . The time $t = \tau$ is indicated by a vertical solid line, the curve $\text{MSD} = 6D_\infty t$ is depicted as a horizontal solid line.

IV. THE SHEAR INERTIA MODEL

To model the observed shear viscosity spectrum of pure water, we consider a general stress-strain relation, which links off-diagonal components of stress and strain rate tensors at $\mathbf{k} = 0$ via [8]

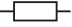

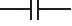



$$\tilde{\sigma}_{\alpha\beta}(\omega) = 2(-i\omega)\tilde{\eta}(\omega)\tilde{\epsilon}_{\alpha\beta}(\omega) \quad \alpha \neq \beta, \quad (14)$$

cf., Eq. (2). This relation is analogous to electrical circuit theory, where one is interested in the total complex impedance $\tilde{Z}(\omega)$ of a circuit, which links time-dependent voltage U and time-dependent current I via [39] $\tilde{U}(\omega) = \tilde{Z}(\omega)\tilde{I}(\omega)$. In analogy to electrical networks, we use Eq. (14) to model the total complex shear viscosity $\tilde{\eta}(\omega)$ of a viscoelastic network [8].

The building blocks for electrical circuits are resistor, capacitor and inductor, and each of them has a characteristic complex impedance $\tilde{Z}(\omega)$, shown in the left column of Table I. In viscoelasticity, usually only viscoelastic analogues of the resistor and the capacitor, but not of the inductor, are considered. The viscoelastic analog of the resistor is the dashpot (both resistor and dashpot dissipate energy), while the viscoelastic analog of the capacitor is the spring (both capacitor and spring can store energy). The rules for calculating the total viscosity of a viscoelastic network, built up by serial and parallel combination of viscoelastic building blocks, are given in Table II [8].

In Figs. 4(a), 4(b), we illustrate the viscoelastic response of two standard viscoelastic materials [8]. The Kelvin–Voigt material, shown in Fig. 4(a), is a parallel combination of a dashpot (viscosity η_0) and a spring (elastic modulus K); it has a complex viscosity $\tilde{\eta}(\omega) = \eta_0 + K/(-i\omega)$,

TABLE I. Electrical and viscoelastic circuit elements.

Electrical circuit		Viscoelastic network	
Building block	$\tilde{Z}(\omega)$	$\tilde{\eta}(\omega)$	Building block
Resistor	 R	η_0	 Dashpot
Capacitor	 $(-i\omega C)^{-1}$	$K(-i\omega)^{-1}$	 Spring
Inductor	 $-i\omega L$	$-i\omega L$	 Shear inertia

and models a viscoelastic solid. The Maxwell material, defined in Eq. (13) and shown in Fig. 4(b), is a serial combination of a dashpot and a spring, and models a viscoelastic fluid; the dashpot viscosity η_0 and spring elastic modulus K are related to the relaxation timescale τ via $\tau = \eta_0/K$.

As can be seen from Figs. 4(a), 4(b), both Kelvin–Voigt and Maxwell model do not exhibit a real part of the complex viscosity that is increasing as a function of frequency. To model the pure water spectrum, and in particular the non-monotonic real part of the viscosity in Fig. 1(a), we introduce the viscoelastic analog of the inductor, which we denote by a circle containing a curved arrow, see right column of Table I. This new circuit element models stress generated by shear acceleration. Indeed, substituting $\tilde{\eta}(\omega) = -i\omega L$ into Eq. (14) and using Eq. (3), it follows that

$$\sigma_{\alpha\beta} = 2L\ddot{\epsilon}_{\alpha\beta} = L\left(\frac{\partial \dot{v}_\alpha}{\partial x_\beta} + \frac{\partial \dot{v}_\beta}{\partial x_\alpha}\right), \quad (15)$$

meaning that the stress is proportional to the shear acceleration. Substituting Eq. (15) into the momentum conservation Eq. (1), the resulting force can be interpreted as contributing an effective induced mass due to velocity gradients in the fluid. A possible microscopic origin of such an effect is the coupling between shear and rotational degrees of freedom of individual fluid particles (vorticity-spin coupling [40]).

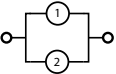
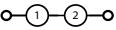
Using the shear inertia circuit element, we consider the viscoelastic network shown in Fig. 4(c), which we call the shear inertia model. As we show now, this is a generalization of the Maxwell model that includes shear inertial effects. Using the viscosities of the individual network elements, cf., Table I, and the combination rules, cf., Table II, the total viscosity of the shear inertia model in Fig. 4(c) is found to be

$$\tilde{\eta}(\omega) = \eta_0 \frac{1 + (-i\omega)\tau_m}{1 + (-i\omega)\tau_0^2/\tau_m + (-i\omega)^2\tau_0^2}, \quad (16)$$

where $\tau_m = L/\eta_0$, $\tau_0^2 = L/K$. From Eq. (16) it can be seen that this is an extension of the Maxwell model, Eq. (13), which is recovered in the limit $\omega\tau_m \rightarrow 0$, $\omega\tau_0 \rightarrow 0$, at finite $\omega\tau_0^2/\tau_m \equiv \omega\tau$.

An important difference between the Maxwell and the shear inertia model is that the latter features a non-monotonic real part in the complex viscosity; from equating its derivative

TABLE II. Combination rules for viscoelastic networks [8].

Combination	Stresses & Strains	Formula for $\tilde{\eta}_{\text{tot}}(\omega)$
Parallel 	$\sigma_{\text{tot}} = \sigma_1 + \sigma_2$ $\epsilon_{\text{tot}} = \epsilon_1 = \epsilon_2$	$\tilde{\eta}_{\text{tot}}(\omega) = \tilde{\eta}_1(\omega) + \tilde{\eta}_2(\omega)$
Serial 	$\sigma_{\text{tot}} = \sigma_1 = \sigma_2$ $\epsilon_{\text{tot}} = \epsilon_1 + \epsilon_2$	$\tilde{\eta}_{\text{tot}}(\omega) = (\tilde{\eta}_1^{-1}(\omega) + \tilde{\eta}_2^{-1}(\omega))^{-1}$

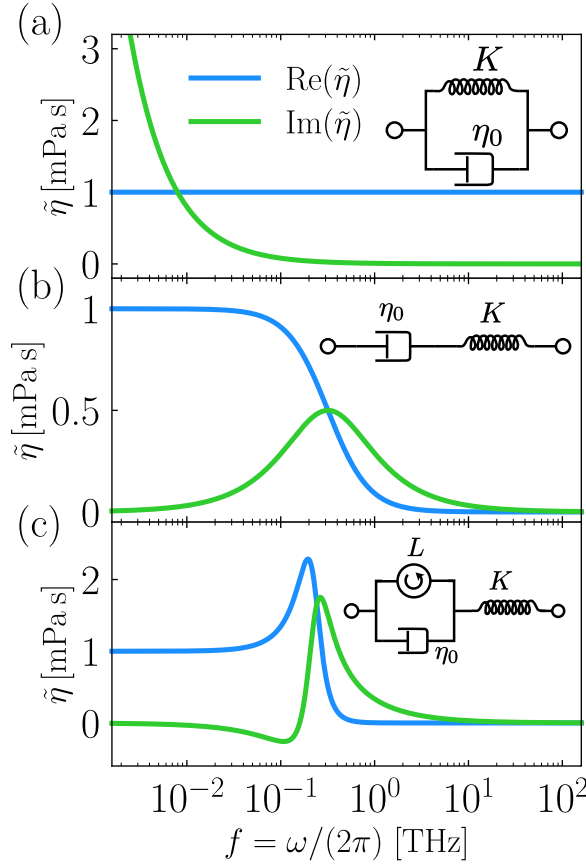


FIG. 4. Complex viscosities of viscoelastic materials. (a) Complex viscosity of a Kelvin–Voigt model, $\tilde{\eta}(\omega) = \eta_0 + K/(-i\omega)$, with $\eta_0 = 1$ mPa s, $K = 5 \times 10^{10}$ mPa. (b) Complex viscosity of a Maxwell model, Eq. (13), with $\eta_0 = 1$ mPa s, $K = 2 \times 10^{12}$ mPa. (c) Complex viscosity of a shear inertia model, Eq. (16), with $\eta_0 = 1$ mPa s, $K = 2 \times 10^{12}$ mPa s, $L = 10^{-12}$ mPa s².

with zero, it follows that the real part of $\tilde{\eta}(\omega)$ defined by Eq. (16) is non-monotonic if and only if

$$\left(\frac{\tau_0}{\tau_m}\right)^2 = \frac{\eta_0^2}{KL} < 1. \quad (17)$$

In Fig. 4(c), we show the complex viscosity of the shear inertia model for parameters $\eta_0 = 1$ mPa s, $K = 2 \times 10^{12}$ mPa s, $L = 10^{-12}$ mPa s². In the low-frequency limit the viscosity spectrum approaches that of a Maxwell model, with constant real part and negligible imaginary part. Also, as in the Maxwell model, both real and imaginary parts vanish in the high frequency limit. However, different from the Maxwell model, the real part of the viscosity is non-monotonic and has a maximum, while the imaginary part is negative for small frequencies. A negative elastic response accompanied by a peak in viscous damping has been observed in acoustic metamaterials before, where it emerges as an effective viscoelastic response due to localized excitable structures within the medium [41,42]; this supports our suggestion that a possible microscopic origin of the shear inertia building block is the coupling between shear and intramolecular rotational degrees of freedom of individual fluid molecules.

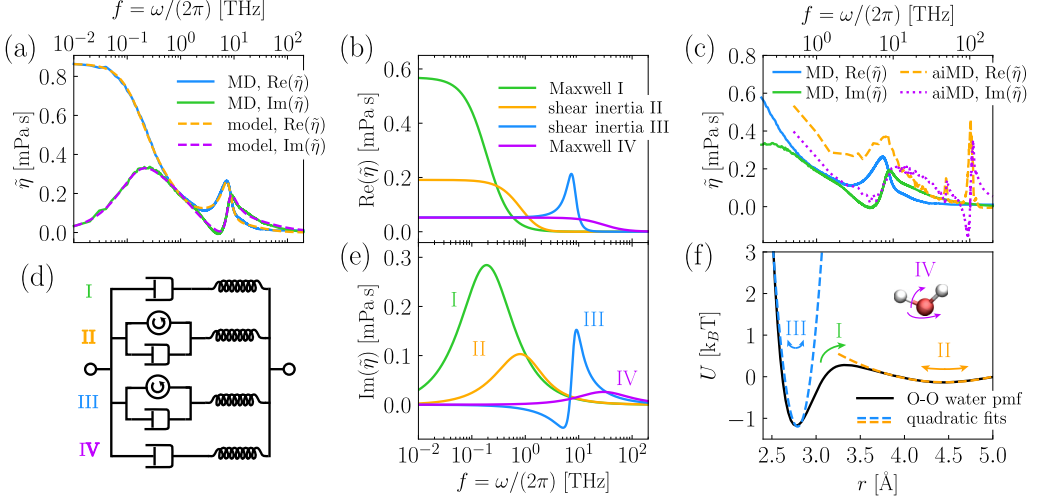


FIG. 5. Viscosity spectrum of pure water. (a): Complex viscosity $\tilde{\eta}$ from MD simulations of TIP4P/2005 water, calculated using Eq. (8), together with a fit of the viscoelastic network shown in subplot (d) with complex viscosity Eq. (18). The fitting parameters are given in Table III. (b), (e): Real and imaginary parts of the individual constituents of the fitted viscosity from subplot (a); (c): Complex viscosity $\tilde{\eta}$ from MD simulations of TIP4P/2005 water (replot of subplot (a)), together with the viscosity calculated from *ab initio* molecular dynamics (aiMD) simulations using Eq. (10) at finite $k = 4.016 \text{ nm}^{-1}$. (d): Viscoelastic network used for modeling the shear response of pure water. The viscoelastic network is a parallel combination of two shear inertia models and two Maxwell models, the resulting complex viscosity is given by Eq. (18); (f): Black line: Potential of mean force $U(r)$ for the oxygen-oxygen distance in TIP4P/2005 water. Blue and yellow lines: Harmonic potentials, fitted around the first and second minima of the pmf. The colored arrows indicate the microscopic interpretation of the constituents of the viscoelastic model shown in subplot (d), namely escape from the nearest neighbor pmf minimum (I), oscillations around the minima (II, III) and librations of individual water molecules (IV).

V. A VISCOELASTIC MODEL FOR PURE WATER AND ITS MICROSCOPIC INTERPRETATION

To model the pure water spectrum, we employ a parallel combination of two Maxwell models and two shear inertia models, illustrated in Fig. 5(d). The total complex viscosity of this network is given by

$$\begin{aligned} \tilde{\eta}(\omega) = & \sum_{j=\text{II,III}} \eta_{0,j} \frac{1 - i\omega\tau_{m,j}}{1 - i\omega\tau_{0,j}^2/\tau_{m,j} - \omega^2\tau_{0,j}^2} + \\ & + \sum_{j=\text{I,IV}} \frac{\eta_{0,j}}{1 - i\omega\tau_j}. \end{aligned} \quad (18)$$

The result of a fit of this model to the MD data is shown in Fig. 5(a), the resulting parameters are given in Table III. As Fig. 5(a) demonstrates, this viscoelastic network is able to reproduce the MD spectrum very well. In Figs. 5(b), 5(e), we additionally show the individual terms of Eq. (18).

For some applications it might be more useful to consider the real-space memory kernel $\eta(t)$ corresponding to Eq. (18), which is why we give and plot $\eta(t)$ in the SM [26]. Furthermore, we show in the SM [26] that fitting three Maxwell models and one shear inertia model yields results of similar quality to our fit Eq. (18). Our choice of two Maxwell models and two shear inertia models is mainly motivated by the microscopic interpretation of the four relaxation modes by which a given strain rate creates stresses, as discussed in the remainder of this section.

TABLE III. Parameters for the viscoelastic model Eq. (18), resulting from a fit to results for TIP4P/2005 water, cf., Figs. 5(a)–5(c), 5(e). Timescales are converted to frequencies via $f = (2\pi\tau)^{-1}$ for ease of comparison with Fig. 5.

Parameter	Value	Interpretation
$\eta_{0,I}$	0.568 mPa s	HB network
$(2\pi\tau_I)^{-1}$	0.19 THz	topology changes
$\eta_{0,II}$	0.19 mPa s	O-O-O vibrations
$(2\pi\tau_{m,II})^{-1}$	2.68 THz	(HB bending)
$(2\pi\tau_{0,II})^{-1}$	1.27 THz	
$\eta_{0,III}$	0.053 mPa s	O-O vibrations
$(2\pi\tau_{m,III})^{-1}$	4.03 THz	(HB stretching)
$(2\pi\tau_{0,III})^{-1}$	7.83 THz	
$\eta_{0,IV}$	0.052 mPa s	Librations
$(2\pi\tau_{IV})^{-1}$	28.92 THz	

We first calculate the radial distribution function $g(r)$ for oxygen atoms and use it to obtain the potential of mean force (pmf) $U(r)$ for the effective oxygen-oxygen interaction via Boltzmann inversion,

$$U(r) = -k_B T \ln [g(r)], \quad (19)$$

see Fig. 5(f). The pmf shows a primary minimum at an oxygen-oxygen distance of approximately $r \approx 2.8 \text{ \AA}$, corresponding to two hydrogen-bonded nearest neighbor water molecules.

In Sec. III we already showed that Maxwell model I, which in Fig. 5(e) shows a peak in the elastic response at $f \approx 0.2 \text{ THz}$, corresponds to rearrangements of individual fluid molecules. For water, this elastic response has been observed experimentally [7]. Mean first-passage times for the dissociation of a water-water pair from the nearest neighbor pmf minimum for simulated SPC/E water are about [36,43] $\tau_{\text{escape}} \approx 4\text{--}5 \text{ ps}$, which translates to frequencies $1/\tau_{\text{escape}} \approx 0.20\text{--}0.25 \text{ THz}$, in very good agreement with the position of the leftmost peak of the imaginary part in Fig. 5(a), 5(c). A comparison of these SPC/E results with our TIP4P/2005 data is legitimate, because, as we show in the SM [26], the viscosity spectrum of SPC/E water is very similar to the TIP4P/2005 spectrum shown in Fig. 5. In particular the lowest-frequency peak is located at a comparable frequency.

The second feature we interpret microscopically is the shear inertia model III. In Table IV we give frequencies for various modes in liquid water obtained from experiments and simulations. Both Raman- and infrared (IR) spectroscopy find hydrogen bond stretch vibrations at frequencies $f \approx 4.5\text{--}5.5 \text{ THz}$, while simulation works find them slightly higher, at 6 THz (aiMD [44]) and 6.9 THz (TIP4P/2005f [45]), respectively. These frequencies are comparable to the position of the spectral features described by shear inertia model III in Figs. 5(b) and 5(e), which suggests that the microscopic origin of the corresponding resonance in our spectrum are vibrations of hydrogen-

TABLE IV. Frequencies for various resonances of liquid water. All frequencies are given in THz.

	Raman spectroscopy [15]	Infrared spectroscopy (IR) [16,17]	IR from aiMD [44]	IR from MD (TIP4P/2005f) [45]	Viscosity from MD (TIP4P/2005, this work)
O-O vibrations (HB stretching)	4.7	$\approx 5.1\text{--}5.5$	6.0	6.9	6.7
O-O-O vibrations (HB bending)	2.0	1.5	2.4	1.5	1.7
Librations	$\approx 12\text{--}24$	$\approx 12\text{--}21$	$\approx 18\text{--}24$	≈ 17	28.9

bonded water pairs around the minimum at $r \approx 2.8 \text{ \AA}$ in Fig. 5(f). More explicitly, multiplying Eq. (16) by the denominator of the right-hand side, and performing an inverse Fourier transform, it can be seen that $\eta(t)$ is the solution of the damped harmonic oscillator equation

$$\ddot{\eta}(t) + \frac{1}{\tau_m} \dot{\eta}(t) + \frac{1}{\tau_0^2} \eta(t) = 0 \quad (20)$$

with initial conditions $\eta(0) = \eta_0 \tau_m / \tau_0^2$, $\dot{\eta}(t) = 0$. With the fitted parameters for shear inertia model III, given in Table III, it follows that the damped harmonic oscillator solution to Eq. (20) is indeed an underdamped oscillation, which is why an extension of the standard (overdamped) Maxwell model is required to describe this feature. The resonance frequency of the underdamped harmonic oscillator defined by Eq. (20) evaluates to

$$f_r = \frac{1}{2\pi} \sqrt{\frac{1}{\tau_0^2} - \frac{1}{4\tau_m^2}} \approx 6.7 \text{ THz}, \quad (21)$$

which is close to the values for hydrogen–bond stretching vibrations found in the literature, see Table IV. Furthermore, the timescales τ_0 , τ_m , obtained from the fitted shear inertia model III are in agreement with the intuitive picture of a hydrogen–bonded water pair oscillating around the first minimum of the pmf shown in Fig. 5(f), as we will explain next. To proceed, we note that according to Eq. (20), the frequency for undamped oscillations obtained from the shear inertia model III fit is given by

$$f_{\text{osc,III}} = \frac{1}{2\pi \tau_{0,\text{III}}} \approx 7.83 \text{ THz}, \quad (22)$$

which is not very different from the result including damping in Eq. (21). The frequency Eq. (22) is comparable to the frequency for an undamped harmonic oscillation of a bonded water pair around the first minimum of the pmf,

$$f_{\text{ho}} = \frac{1}{2\pi} \sqrt{\frac{k}{m}} \approx 8.82 \text{ THz}, \quad (23)$$

where the force constant $k = 110.85 k_B T / \text{\AA}^2$ is obtained by fitting a quadratic potential

$$U(r) = U(r_0) + \frac{k}{2} (r - r_0)^2 \quad (24)$$

to the minimum at $r_0 \approx 2.8 \text{ \AA}$, cf., the blue dashed curve in Fig. 5(f), and for m we use the reduced water mass $m = m_{\text{water}}/2 = 9 \text{ amu}$, appropriate for relative oscillations of two rigid water molecules. Considering a damped harmonic oscillator equation for this relative oscillation of two hydrogen-bonded water molecules furthermore allows to estimate the effective friction coefficient γ for a vibrating water molecule pair within the hydrogen bond network. More explicitly, for a damped harmonic oscillator equation $m\ddot{\Delta r} + \gamma\dot{\Delta r} + k\Delta r = 0$, with $\Delta r = r - r_0$ the deviation of the oxygen-oxygen distance of a hydrogen-bonded water pair from the local minimum $r_0 \approx 2.8 \text{ \AA}$, the inertial decay timescale is given by $\tau_m = m/\gamma$. Equating this timescale with the corresponding inertial decay timescale in Eq. (20), we estimate

$$\gamma = m/\tau_m \approx 2\pi \times 9 \text{ amu} \times 4.03 \text{ THz} \approx 0.38 \frac{\text{pN ns}}{\text{nm}}, \quad (25)$$

where again we use $m = m_{\text{water}}/2 = 9 \text{ amu}$. The value obtained in Eq. (25) is almost one order of magnitude smaller than the friction coefficient of a diffusing water molecule, $\gamma \approx 1.62 \text{ pN ns/nm}$ [36], which physically makes sense because a diffusing water molecule is expected to experience more resistance to motion as compared to a particle oscillating within a local potential minimum. Relative oscillations of hydrogen–bonded water molecules contribute to the shear viscosity because of the polarity of an individual water molecule, which couples translation and rotation of individual

molecules within the hydrogen–bond network; indeed, as we show in the SM [26], upon turning off the electrostatic interactions between the water molecules, so that a LJ fluid model is recovered, the shear inertia III feature in the viscosity spectrum disappears. Our microscopic interpretation of shear inertia model III is furthermore consistent with the fact that the peak at about 9 THz disappears as the glycerol mass fraction is increased, cf., Fig. 1, because diffusing glycerol molecules hinder the hydrogen bond network of water [46]. To demonstrate this, we in the SM [26] show the average number of water–water hydrogen bonds per water molecule, which drops by a factor of about 2 as the glycerol mass fraction is increased from 0 to 0.8. We thus conclude that the microscopic origin of shear inertia model III are hydrogen bond vibrations of neighboring water molecules.

Similarly, we interpret shear inertia model II as oscillations around the second minimum of the pmf shown in Fig. 5(f), at around $r_0 \approx 4.5 \text{ \AA}$, corresponding to oxygen–oxygen–oxygen (O–O–O) vibrations within the hydrogen bond network of water. In contrast to shear inertia model III, now the fitted damped harmonic oscillator Eq. (20) is overdamped, so that O–O–O hydrogen bond vibrations are actually overdamped. As we show in the SM [26], using a standard Maxwell model for feature II is also possible. Indeed, approximating the overdamped mode Eq. (16) by a Maxwell model with relaxation timescale $\tau = \tau_0^2/\tau_m$, we find a resonance frequency $f_r \approx (2\pi\tau)^{-1} \approx 1.7 \text{ THz}$, which is close to the literature values for hydrogen–bond bending vibrations [15–17,45], see Table IV. While the fitted shear inertia model II describes an overdamped oscillator, employing a shear inertia model instead of a Maxwell model allows us to estimate the effective friction coefficient for O–O–O vibrations, as

$$\gamma \sim m/\tau_m \approx 2\pi \times 9 \text{ amu} \times 2.68 \text{ THz} \approx 0.25 \frac{\text{pN ns}}{\text{nm}}, \quad (26)$$

where we again use the reduced mass $m = m_{\text{water}}/2 = 9 \text{ amu}$ as an estimate for the inertia, based on the picture that during O–O–O bending vibrations, the middle molecule does not move significantly. This value for the molecular friction γ is of the same order of magnitude as the one obtained for shear inertia model III, cf., Eq. (25), and is also considerably smaller than the friction coefficient of a diffusing water molecule, $\gamma \approx 1.62 \text{ pN ns/nm}$ [36]. Note finally that also for shear inertia model II, the frequencies obtained from the fit are in agreement with expectations from the pmf in Fig. 5(f). Indeed, a quadratic fit to the second minimum of the pmf, shown as the yellow dashed line in the figure, leads to an undamped oscillation frequency

$$f_{\text{ho}} = \frac{1}{2\pi} \sqrt{\frac{k}{m}} \approx 0.81 \text{ THz}, \quad (27)$$

where as above we use the reduced mass $m = m_{\text{water}}/2$ as an estimate for the inertia. The fitted shear inertia model II yields the comparable frequency

$$f_{\text{osc,II}} = \frac{1}{2\pi\tau_{0,\text{II}}} \approx 1.27 \text{ THz}. \quad (28)$$

While we here base our assignment of shear inertial model II to O–O–O vibrations on comparing literature values for the frequency of this oscillation to timescales obtained from the O–O pmf shown in Fig. 5(f), a more direct assignment would be possible by analyzing the normal modes of hydrogen-bonded water triples, and isolating the O–O–O vibrations [19]. Such an analysis is beyond the scope of the present paper and might be undertaken in a future work.

The highest frequency features, described by Maxwell model IV, we interpret as librational excitations, i.e. rotational vibrations of individual water molecules within the force field of their surrounding molecules. To show this, we in the SM consider orientational spectra calculated for individual water molecules, which show a peak at frequencies comparable to the elastic response frequency of Maxwell model IV [26]. Note that spectroscopy locates such vibrations at frequencies considerably higher than O–O vibrations, cf., Table IV. That inertial effects can be neglected here

is consistent with the fact that for the rotational motion of SPC/E water, inertia starts to dominate only at much higher frequencies, namely at around 90 THz [47].

In addition to our results obtained from TIP4P/2005, a classical rigid water model, we calculate the viscosity spectrum for pure water also from from aiMD simulations, see SM for details [26]. For the aiMD data, we use Eq. (10) at finite $k = 4.016 \text{ nm}^{-1} = 2\pi/L$, where $L = 1.56 \text{ nm}$ is the edge length of the cubic simulation box. A comparison of aiMD and TIP4P/2005 spectra (the latter as before at $k = 0$) is shown in Fig. 5(c). Qualitative deviations between the spectra appear at frequencies above 50 THz, where intramolecular degrees of freedom [15,44] (OH stretching, OH bending), which are not accounted for in a rigid water model, become relevant. Up to these frequencies, however, the spectra show the same features, in particular the peak at around 9 THz with its high-frequency shoulder is present in both the aiMD and the force-field MD spectra; this confirms that the spectrum obtained from force-field MD is indeed accurate up to about 50 THz. This finding is in agreement with the recent comparison of aiMD and force-field MD results for the linear absorption of pure water from 1 MHz to 100 THz [18].

VI. CONCLUSIONS

In this work we calculate the viscoelastic properties of both pure water and water-glycerol mixtures from force-field MD simulations. For water-glycerol mixtures, we find very good agreement of the viscosity and the relaxation time with experimental data [6,30], for pure water our spectrum agrees both with previous theoretical results [10,38], and with a spectrum calculated from aiMD simulations at finite wave numbers. Using an extension of the Maxwell model for viscoelastic fluids, which includes shear inertial effects, we propose a functional form for the shear viscosity of pure water that is able to describe the force-field MD spectrum over the entire frequency range considered. By comparing to Raman and IR spectra, as well as to other observables calculated from our MD data, we subsequently identify the molecular processes underlying this spectrum as water network topology changes, collective vibrations of three water molecules, hydrogen-bond stretch vibrations of water pairs, and librational excitations of individual water molecules.

The viscoelastic circuit we propose describes the short-time non-Markovian behavior of water in the picosecond regime, where the standard Newtonian fluid stress-strain relation becomes a poor approximation to the actual dynamics of the fluid. Only the viscoelastic response at the longest timescales discussed here has been measured until now [6,7], so that our results present a challenge for future experimental investigation.

Note that recently it was argued that phonons can travel along the hydrogen bond network, and that elastic peaks in the range of tens of THz should be interpreted as such phonons [48], which is consistent with our interpretation of these peaks as bond vibrations. At timescales smaller than those of water network topology changes, one could think of water as a static network, possibly with defects. Starting from a tetrahedral lattice and calculating the corresponding viscoelastic response [49] might yield further insights into the high-frequency viscoelastic properties of water.

To obtain an even more detailed picture of the breakdown of the Newtonian fluid picture at small scales, a possible next step would be to also systematically study short-distance non-local effects by considering viscosity kernels at finite wave vector k [10,50], or to combine analytical methods with simulations [51,52]. One particularly interesting avenue will be relating the viscoelastic response of the medium to a generalized Langevin model for a single fluid molecule [27,53].

ACKNOWLEDGMENTS

We acknowledge funding from the DFG via SFB 1114, Project No. 235221301, Project C2. Work was funded in part by the European Research Council under the EU's Horizon 2020 Program, Grant No. 740269.

- [1] Biman Bagchi, *Water in Biological and Chemical Processes: From Structure and Dynamics to Function* (Cambridge University Press, Cambridge, UK, 2013).
- [2] G. W. Robinson, S. Singh, S.-B. Zhu, and M. W. Evans, *Water in Biology, Chemistry and Physics: Experimental Overviews and Computational Methodologies*, Vol. 9 (World Scientific, Singapore, 1996).
- [3] L. D. Landau and E.M. Lifshitz, *Fluid Mechanics* (Butterworth-Heinemann, Oxford, UK, 1987).
- [4] D. J. Acheson, *Elementary Fluid Dynamics* (Clarendon Press, Oxford, UK, 1990).
- [5] G. K. Batchelor, *An Introduction to Fluid Dynamics* (Cambridge University Press, Cambridge, UK, 2000).
- [6] W. M. Slie, A. R. D. Jr, and T. A. Litovitz, Ultrasonic shear and longitudinal measurements in aqueous glycerol, *J. Chem. Phys.* **44**, 3712 (1966).
- [7] M. Pelton, D. Chakraborty, E. Malachosky, P. Guyot-Sionnest, and J. E. Sader, Viscoelastic Flows in Simple Liquids Generated by Vibrating Nanostructures, *Phys. Rev. Lett.* **111**, 244502 (2013).
- [8] R. M. Christensen, *Theory of Viscoelasticity* (Courier Corporation, North Chelmsford, MA, 2003).
- [9] N. M. Lacevic and J. E. Sader, Viscoelasticity of glycerol at ultra-high frequencies investigated via molecular dynamics simulations, *J. Chem. Phys.* **144**, 054502 (2016).
- [10] I. Omelyan, I. Mryglod, and M. Tokarchuk, Wavevector- and frequency-dependent shear viscosity of water: the modified collective mode approach and molecular dynamics calculations, *Condens. Matter Phys.* **8**, 25 (2005).
- [11] T. J. O’Sullivan, S. K. Kannam, D. Chakraborty, B. D. Todd, and J. E. Sader, Viscoelasticity of liquid water investigated using molecular dynamics simulations, *Phys. Rev. Fluids* **4**, 123302 (2019).
- [12] L. Bocquet and E. Charlaix, Nanofluidics, from bulk to interfaces, *Chem. Soc. Rev.* **39**, 1073 (2010).
- [13] P. V. Ruijgrok, P. Zijlstra, A. L. Tchebotareva, and M. Orrit, Damping of acoustic vibrations of single gold nanoparticles optically trapped in water, *Nano Lett.* **12**, 1063 (2012).
- [14] A. Cunsolo, G. Ruocco, F. Sette, C. Masciovecchio, A. Mermet, G. Monaco, M. Sampoli, and R. Verbeni, Experimental Determination of the Structural Relaxation in Liquid Water, *Phys. Rev. Lett.* **82**, 775 (1999).
- [15] D. M. Carey and G. M. Korenowski, Measurement of the raman spectrum of liquid water, *J. Chem. Phys.* **108**, 2669 (1998).
- [16] H. R. Zelsmann, Temperature dependence of the optical constants for liquid H₂O and D₂O in the far ir region, *J. Mol. Struct.* **350**, 95 (1995).
- [17] H. J. Liebe, G. A. Hufford, and T. Manabe, A model for the complex permittivity of water at frequencies below 1 THz, *Int. J. Infrared Millimeter Waves* **12**, 659 (1991).
- [18] S. Carlson, F. N. Brünig, P. Loche, D. J. Bonthuis, and R. R. Netz, Exploring the absorption spectrum of simulated water from MHz to infrared, *J. Phys. Chem. A* **124**, 5599 (2020).
- [19] R. Schulz, Y. von Hansen, J. O. Daldrop, J. Kappler, F. Noé, and R. R. Netz, Collective hydrogen-bond rearrangement dynamics in liquid water, *J. Chem. Phys.* **149**, 244504 (2018).
- [20] R. Zwanzig, Time-correlation functions and transport coefficients in statistical mechanics, *Annu. Rev. Phys. Chem.* **16**, 67 (1965).
- [21] J.-P. Hansen and I. R. McDonald, *Theory of Simple Liquids* (Elsevier, Amsterdam, 1990).
- [22] P. J. Davis and D. J. Evans, Comparison of constant pressure and constant volume nonequilibrium simulations of sheared model decane, *J. Chem. Phys.* **100**, 541 (1994).
- [23] D. J. Evans and G. Morriss, *Statistical Mechanics of Nonequilibrium Liquids* (Cambridge University Press, Cambridge, UK, 2008).
- [24] M. Mondello and G. S. Grest, Viscosity calculations of n-alkanes by equilibrium molecular dynamics, *J. Chem. Phys.* **106**, 9327 (1997).
- [25] T. Chen, B. Smit, and A. T. Bell, Are pressure fluctuation-based equilibrium methods really worse than nonequilibrium methods for calculating viscosities? *J. Chem. Phys.* **131**, 246101 (2009).
- [26] See Supplemental Material at <http://link.aps.org/supplemental/10.1103/PhysRevFluids.5.103301> for more details on theoretical derivations and further analysis of the numerical data. The Supplemental Material includes citations to Refs. [54–64].
- [27] B. Kowalik, J. O. Daldrop, J. Kappler, J. C. F. Schulz, A. Schlaich, and R. R. Netz, Memory-kernel extraction for different molecular solutes in solvents of varying viscosity in confinement, *Phys. Rev. E* **100**, 012126 (2019).

- [28] S. Pronk, S. Páll, R. Schulz, P. Larsson, P. Bjelkmar, R. Apostolov, M. R. Shirts, J. C. Smith, P. M. Kasson, D. van der Spoel, B. Hess, and E. Lindahl, Gromacs 4.5: A high-throughput and highly parallel open source molecular simulation toolkit, *Bioinformatics* **29**, 845 (2013).
- [29] A. K. Malde, L. Zuo, M. Breeze, M. Stroet, D. Poger, P. C. Nair, C. Oostenbrink, and A. E. Mark, An automated force field topology builder (atb) and repository: Version 1.0, *J. Chem. Theory Comput.* **7**, 4026 (2011).
- [30] N.-S. Cheng, Formula for the viscosity of a glycerol-water mixture, *Ind. Eng. Chem. Res.* **47**, 3285 (2008).
- [31] S. Tazi, A. Bořan, M. Salanne, V. Marry, P. Turq, and B. Rotenberg, Diffusion coefficient and shear viscosity of rigid water models, *J. Phys.: Condens. Matter* **24**, 284117 (2012).
- [32] R. Zwanzig and R. D. Mountain, High-frequency elastic moduli of simple fluids, *J. Chem. Phys.* **43**, 4464 (1965).
- [33] J. Frenkel, *Kinetic Theory of Liquids* (Oxford University Press, Oxford, UK, 1946).
- [34] T. Iwashita, D. M. Nicholson, and T. Egami, Elementary Excitations and Crossover Phenomenon in Liquids, *Phys. Rev. Lett.* **110**, 205504 (2013).
- [35] J. Ashwin and A. Sen, Microscopic Origin of Shear Relaxation in a Model Viscoelastic Liquid, *Phys. Rev. Lett.* **114**, 055002 (2015).
- [36] Y. von Hansen, F. Sedlmeier, M. Hinczewski, and R. R. Netz, Friction contribution to water-bond breakage kinetics, *Phys. Rev. E* **84**, 051501 (2011).
- [37] V. V. Palyulin, C. Ness, R. Milkus, R. M. Elder, T. W. Sirk, and A. Zaccone, Parameter-free predictions of the viscoelastic response of glassy polymers from non-affine lattice dynamics, *Soft Matter* **14**, 8475 (2018).
- [38] A. V. Straube, B. G. Kowalik, R. R. Netz, and F. Höfling, Rapid onset of molecular friction in liquids bridging between the atomistic and hydrodynamic pictures, *Commun. Phys.* **3**, 126 (2020).
- [39] C. Alexander and M. Sadiku, *Fundamentals of Electric Circuits* (McGraw Hill Higher Education, New York, NY, 2008).
- [40] D. J. Bonthuis, D. Horinek, L. Bocquet, and R. R. Netz, Electrokinetics at aqueous interfaces without mobile charges, *Langmuir* **26**, 12614 (2010).
- [41] N. Fang, D. Xi, J. Xu, M. Ambati, W. Srituravanich, C. Sun, and X. Zhang, Ultrasonic metamaterials with negative modulus, *Nat. Mater.* **5**, 452 (2006).
- [42] Y. Wu, Y. Lai, and Z.-Q. Zhang, Elastic Metamaterials with Simultaneously Negative Effective Shear Modulus and Mass Density, *Phys. Rev. Lett.* **107**, 105506 (2011).
- [43] F. Sedlmeier, Y. von Hansen, L. Mengyu, D. Horinek, and R. R. Netz, Water dynamics at interfaces and solutes: Disentangling free energy and diffusivity contributions, *J. Stat. Phys.* **145**, 240 (2011).
- [44] M. Heyden, J. Sun, S. Funkner, G. Mathias, H. Forbert, M. Havenith, and D. Marx, Dissecting the THz spectrum of liquid water from first principles via correlations in time and space, *Proc. Natl. Acad. Sci. USA* **107**, 12068 (2010).
- [45] M. A. González and J. L. F. Abascal, A flexible model for water based on tip4p/2005, *J. Chem. Phys.* **135**, 224516 (2011).
- [46] I. Popov, A. Greenbaum (Gutina), A. P. Sokolov, and Y. Feldman, The puzzling first-order phase transition in water-glycerol mixtures, *Phys. Chem. Chem. Phys.* **17**, 18063 (2015).
- [47] Y. von Hansen, Stochastic Dynamics in Biomolecular Systems, Ph.D. thesis, Freie Universität Berlin, 2014.
- [48] D. C. Elton and M. Fernández-Serra, The hydrogen-bond network of water supports propagating optical phonon-like modes, *Nat. Commun.* **7**, 10193 (2016).
- [49] Y. von Hansen, S. Rode, and R. R. Netz, Convolution theory for dynamic systems: A bottom-up approach to the viscoelasticity of polymeric networks, *Eur. Phys. J. E* **36**, 137 (2013).
- [50] O. Behrend, R. Harris, and P. B. Warren, Hydrodynamic behavior of lattice Boltzmann and lattice Bhatnagar-Gross-Krook models, *Phys. Rev. E* **50**, 4586 (1994).
- [51] R. Milkus and A. Zaccone, Atomic-scale origin of dynamic viscoelastic response and creep in disordered solids, *Phys. Rev. E* **95**, 023001 (2017).

- [52] R. M. Elder, A. Zaccone, and T. W. Sirk, Identifying nonaffine softening modes in glassy polymer networks: A pathway to chemical design, *ACS Macro Lett.* **8**, 1160 (2019).
- [53] B. Cui, J. Yang, J. Qiao, M. Jiang, L. Dai, Y.-J. Wang, and A. Zaccone, Atomic theory of viscoelastic response and memory effects in metallic glasses, *Phys. Rev. B* **96**, 094203 (2017).
- [54] C. Oostenbrink, A. Villa, A. E. Mark, and W. F. Van Gunsteren, A biomolecular force field based on the free enthalpy of hydration and solvation: The GROMOS force-field parameter sets 53A5 and 53A6, *J. Comput. Chem.* **25**, 1656 (2004).
- [55] M. Parrinello and A. Rahman, Polymorphic transitions in single crystals: A new molecular dynamics method, *J. Appl. Phys.* **52**, 7182 (1981).
- [56] H. J. C. Berendsen, J. R. Grigera, and T. P. Straatsma, The missing term in effective pair potentials, *J. Phys. Chem.* **91**, 6269 (1987).
- [57] T. Darden, D. York, and L. Pedersen, Particle mesh ewald: An $n \cdot \log(n)$ method for ewald sums in large systems, *J. Chem. Phys.* **98**, 10089 (1993).
- [58] J. L. F. Abascal and C. Vega, A general purpose model for the condensed phases of water: Tip4p/2005, *J. Chem. Phys.* **123**, 234505 (2005).
- [59] G. Bussi, D. Donadio, and M. Parrinello, Canonical sampling through velocity rescaling, *J. Chem. Phys.* **126**, 014101 (2007).
- [60] B. J. Palmer, Transverse-current autocorrelation-function calculations of the shear viscosity for molecular liquids, *Phys. Rev. E* **49**, 359 (1994).
- [61] R. Zwanzig, *Nonequilibrium Statistical Mechanics* (Oxford University Press, New York, NY, 2001).
- [62] J. O. Daldrop, M. Saita, M. Heyden, V. A. Lorenz-Fonfria, J. Heberle, and R. R. Netz, Orientation of non-spherical protonated water clusters revealed by infrared absorption dichroism, *Nat. Commun.* **9**, 311 (2018).
- [63] A. Luzar and D. Chandler, Hydrogen-bond kinetics in liquid water, *Nature* **379**, 55 (1996).
- [64] A. Luzar, Resolving the hydrogen bond dynamics conundrum, *J. Chem. Phys.* **113**, 10663 (2000).